14th Australasian Fluid Mechanics Conference
Adelaide University, Adelaide, Australia
10-14 December 2001

Laboratory and Computer Experiments on Turbulent Mixing

Paul E. Dimotakis
Graduate Aeronautical Laboratories of the California Institute of Technology
Pasadena, California 91125, USA

Abstract

This discussion covers some progress in turbulent mixing stemming from experimental, modeling, and direct-numerical simulation (DNS) studies. Topics include the mixing transition, results from DNS studies of the Rayleigh-Taylor instability in miscible fluids, experimental investigations in transverse jets and the assumption of isotropy in turbulence and mixing, and experiments in high-speed shear layers that elucidate some effects of compressibility on the mixed-fluid field.

Introduction

Turbulence remains a scientific challenge, despite sustained and inspired contributions especially during the latter half of the 20th century. Turbulent *mixing* presents particular difficulties because while driven by scalar fluxes typically dominated by large-scale motions, the final, diffusive, molecular-mixing stage occurs at the smallest spatial and temporal scales of the flow, necessitating a correct description of the whole spectrum.

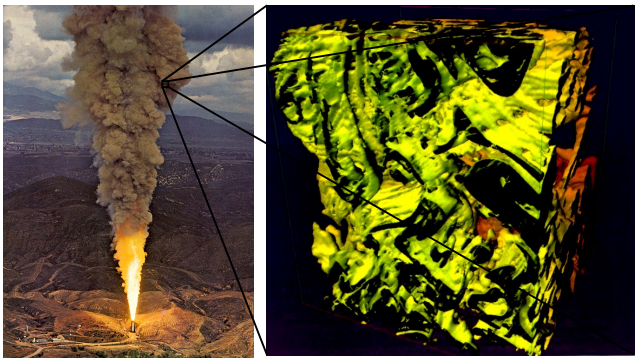

Figure 1 Left: Rocket testing in the Los Angeles hills [3], $Re > 10^8$. Right: LIF measurements of jet-fluid concentration isosurfaces in a turbulent jet in water [4], $Re \cong 10^4$.

The ratio of the largest-to-smallest scales that need to be described is a function of the Reynolds number, *Re*, and Schmidt number ($Sc = \nu/D$) of the flow. Accepting standard scaling [1,2], we have $\lambda_{max}/\lambda_{min} \sim Re^{3/4}Sc^{1/2}$, corresponding to a required dynamic range proportional to Re^3 for gas-phase mixing ($Sc \approx 1$) to describe turbulence (3×¾ for space + ¾ for time). Liquid-phase ($Sc \approx 1000$) mixing is even more challenging. In view of this scaling, it is tempting to ask how low *Re* can be for flow that is representative of *bona fide* turbulence.

Considering the *Re* values of interest, this imposes a daunting task for any investigation, be it experimental or numerical simulation, as the dimensionality of the phenomena and the data required to describe them is very high.

The mixing transition

Turbulent flows exhibit a transition that can be conspicuous, at outer-scale Reynolds numbers, $Re_\delta \equiv \rho U \delta / \mu \geq 1\text{–}2\times10^4$, or a Taylor Reynolds number of $Re_T \equiv \rho\, u' \lambda_T / \mu \geq 100$, where δ is an outer-scale length, U the characteristic velocity that drives the flow, u' the rms velocity, and λ_T the Taylor microscale. The latter provides a criterion where an outer-scale Reynolds number is not appropriate. Where both can be defined, the quoted threshold values are consistent with the general approximate relation, $Re_T \approx (Re_\delta)^{1/2}$. These provide *necessary* but not *sufficient* requirements for this transition; laminar flows, for example, can be encountered at higher *Re*'s yet [5].

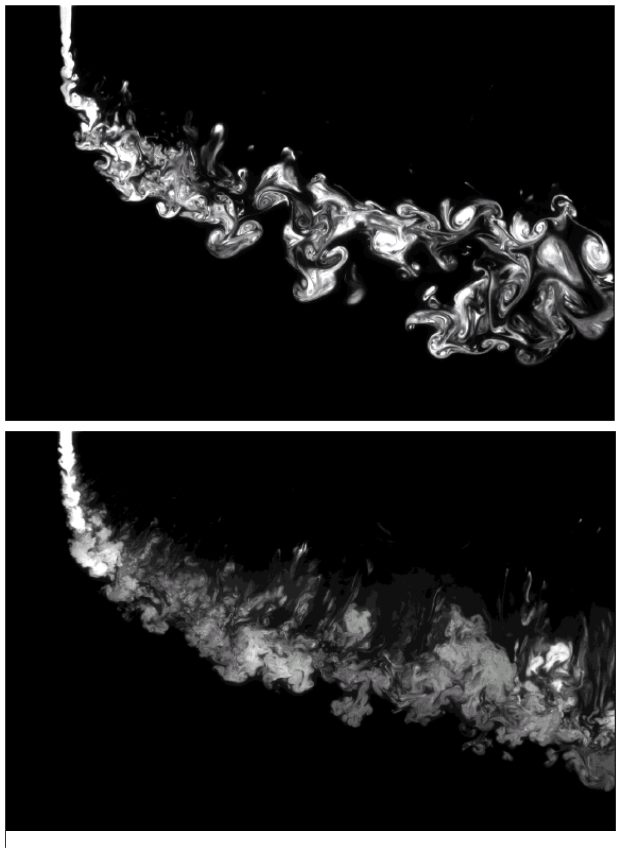

Figure 2 Transverse jet in a uniform free stream, $U_j / U_\infty \approx 10$. Concentration field intensity compensated for mixing with $x^{1/2}$ for visualization purposes Top: $Re = 1000$. Bottom: $Re = 10{,}000$ [6].

An explanation or this transition has been proposed in terms of the need for the existence of inertial-range dynamics, *i.e.*, an inviscid range of scales. This leads to a criterion for a minimum Reynolds number, as noted above, in accord with observations [5].

While this transition was first documented through its effects on mixing, it is a transition of all aspects of the flow and manifests itself in a multitude of ways. As can be seen in figure 2, which illustrates the phenomenon, the qualitative difference between the pre- and post-mixing-transition flow is considerable and easily registered through its effects on the probability-density function of jet-fluid concentration values, for example. Inferences drawn

from pre-transitional flows should be applied with care as such flows are not necessarily representative of high-*Re* flows.

Growth and mixing in Rayleigh-Taylor flows

The Rayleigh-Taylor instability (RTI) occurs whenever fluids of different density are accelerated in a direction opposite that of the density gradient. If the fluids are miscible, species diffusion and mixing, that reduce density differences and hence local forcing, can play a dynamic role.

Recent direct numerical simulations (DNS) of RTI between miscible flows allowed investigations on the growth and mixing in Rayleigh-Taylor instability (RTI) flow [7]. Figure 3 plots the initial perturbation spectra for four numerical simulation runs. The Navier-Stokes equations, with matched fluid viscosities for the two fluids, with $\rho_2/\rho_1 = 3$, were augmented by a species-conservation equation for binary Fickian diffusion. The runs were executed on the Lawrence Livermore Pacific-Blue ASCI machines [7,8]. Cases A, B, and C were solved on a $256^2\times1024$ grid. Case D was solved on a $512^2\times2048$ grid, ran on 1024 processors, and required a year of wall-clock time.

The linear stability analysis dispersion relation, $\sigma(k)$, derives from the theory by Duff *et al.* [9], $\tau = (L/Ag)^{1/2}$, with L the transverse extent of the RTI cell,

$$A \equiv (\rho_2-\rho_1) / (\rho_2+\rho_1) = 0.5, \qquad (1)$$

the Atwood number, and g the acceleration magnitude.

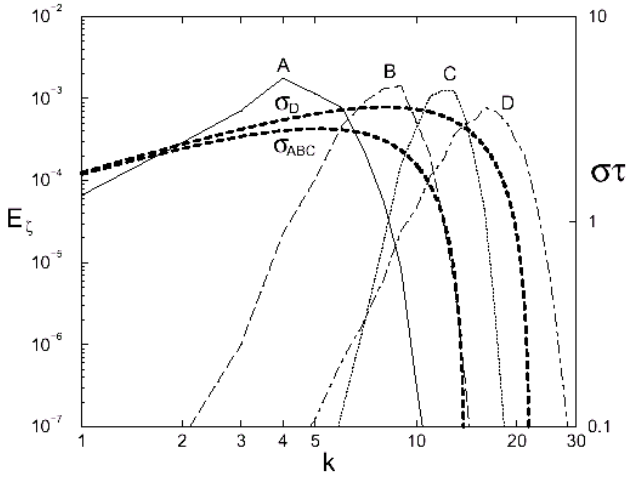

Figure 3 RTI initial perturbation spectra and linear-stability analysis dispersion curves [7,8].

Initial error-function mole-fraction profiles were perturbed by displacing the intermediate isosurface, $X = 1/2$, nominally at $z = 0$, by an amount $\zeta(x,y)$, in units of the initial profile scaling length. The A, B, and C simulations were performed with matched initial perturbation amplitudes, each with a different initial $\zeta(x,y)$ perturbation spectrum (figure 3), but otherwise identical in every other respect.[1] Case D was run with the same boundary conditions, but a lower initial perturbation amplitude, as illustrated below. It was designed to answer whether the A, B, and C results were an artifact of a limited spatial dynamic range and to attain a higher final Reynolds number.

Models of Rayleigh-Taylor instability mixing zone have it growing quadratically in time, following an initial, linear-instability evolution. For a constant acceleration, g, this yields a vertical extent of the RTI mixing zone given by,

$$h = \alpha A g t^2, \qquad (2)$$

where α is taken as an empirical constant, with values in the range, $0.1 < \alpha < 0.7$ [10].

Figure 4 depicts the intermediate mole-fraction isosurface ($X = 1/2$), visualized from the results for Case C [7].

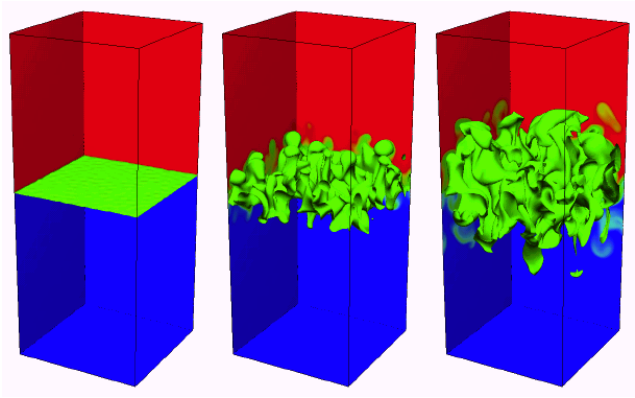

Figure 4 Case C intermediate isosurface, X=1/2 (green), for t/τ = 0.0, 3.44, and 4.63 [7]. Red: pure heavy fluid. Blue: pure light fluid.

Figure 5 plots the computed growth for the four cases. h is defined as the difference in heights, z, where the horizontally averaged mole fraction is given by $X = 0.99$, and 0.01 [7].

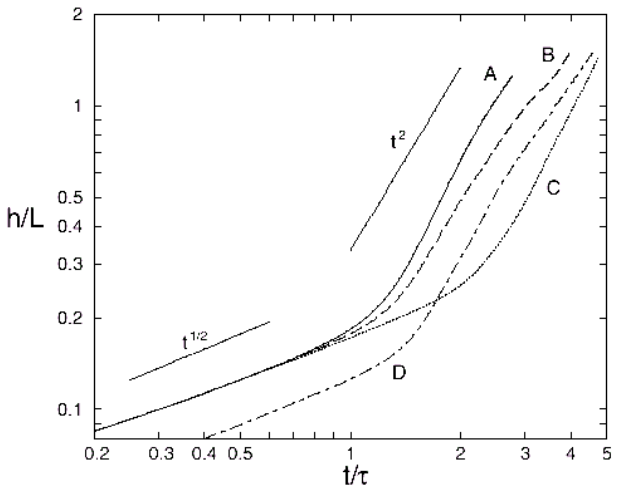

Figure 5 RTI mixing-zone growth.

As can be seen, initial RTI mixed-fluid growth is well-described by diffusion, *i.e.*, $\propto t^{1/2}$. A faster-growth subsequent stage occurs at a different time for each of the three cases, reflecting differences in initial seeding, with breakout times from the diffusive-growth regime in accord with linear-stability theory [8]. While late-time growth for Case C is well represented by a quadratic, Cases A, B, and D exhibit growth with a different time dependence, placing the validity of the empirical model (2) and the hope that a universal value for α may exist in question. Differences in growth between the four cases are large, indicating a high sensitivity to initial conditions.

Even greater differences between the three cases are found in mixing, as measured by the amount of chemical product that would be formed from a stoichiometric chemical reaction between the two miscible fluids being mixed [7]. See figure 6.

[1] A scaling error for σ led to an incorrect plot of the linear-stability-analysis dispersion relation in [7]. It is corrected here and in [8].

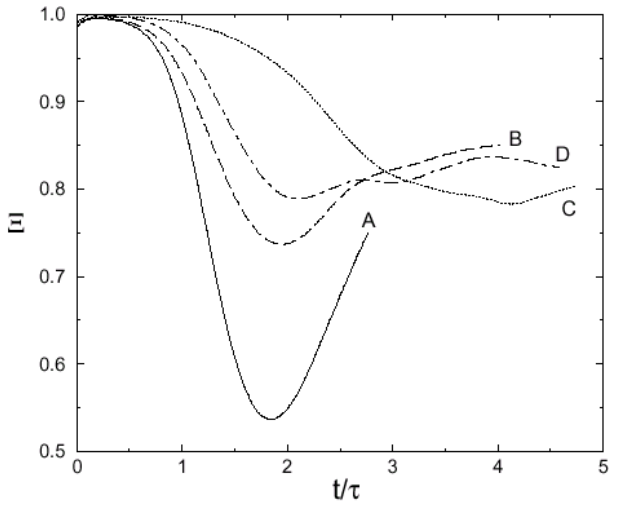

Figure 6 Simulated chemical-product fraction in RTI zone [7].

Differences between the four cases persist to the end of the simulations, to moderate Reynolds numbers,

$$Re_h \equiv \frac{\bar{\rho}\, h \dot{h}}{\mu}, \qquad (3)$$

where $\bar{\rho} = (\rho_1+\rho_2)/2$, with $(Re_h)_{max} = 3700$ for Case C and 5500 for Case D. While these values are below the anticipated mixing transition, the flow evolved over a significant multiple of the initial transverse extent, *i.e.*, $h_{final} / h_{initial} > 10^3$. Other measures also reflect high-*Re* behavior. The chemical-product fraction tends to $\delta_p / h \cong 0.34$ [7], a value very close to that in high-*Re*, gas-phase, chemically reacting shear layers [11]. Taylor microscales computed in the original interface plane ($z = 0$) are non-isotropic, with values along the vertical direction larger than in the horizontal plane, but straddling values measured along the centerline of high-*Re* turbulent jets [7].

Are scalar fields isotropic at small scales?

Turbulence theories often assume that statistical quantities may be approximated as isotropic, yielding a considerable reduction in the tensor components that need to be modeled. This also stems from attention paid to grid turbulence, many aspects of which are (nearly) isotropic, and the fact that most measurements to date have been point measurements. Spatial data are estimated with the aid of Taylor's frozen-turbulence hypothesis, with direct spatial or multi-dimensional information difficult to extract, or infer. The assumption is often that fluxes will be supported by large-scale anisotropy, while small scales may be approximated as isotropic. Yet, an isotropic field cannot support fluxes and, indeed, "…experimental evidence shows that structure functions and the derivative skewness of the scalar field do not follow predictions from isotropy at inertial and dissipative scales, in the presence of a mean scalar gradient." [12 and references therein]

These issues were further investigated in experiments on transverse jets [6]. Transverse jets are important in a variety of turbulent mixing and combustion contexts. They are relied upon to disperse pollutants from stacks in the atmosphere, sometimes used for effluent discharge in the ocean, and are a candidate fuel-injection configuration for high-speed air-breathing propulsion devices, such as SCRAMJETs, for example.

In the transverse-jet experiments, cuts in planes perpendicular to the streamwise direction permitted spatial scalar spectra and other scalar-field statistics to be compiled, at a fixed x / d_j station.

Figure 7 Jet -fluid concentration for a transverse jet in a uniform freestream (cf. figure 2), at $x / d_j = 50$. Top: $Re = 1000$. Bottom: $Re = 10{,}000$ [6].

Measurements were in the mid-span, streamwise plane (figure 2), and the flow-transverse plane (figure 7).

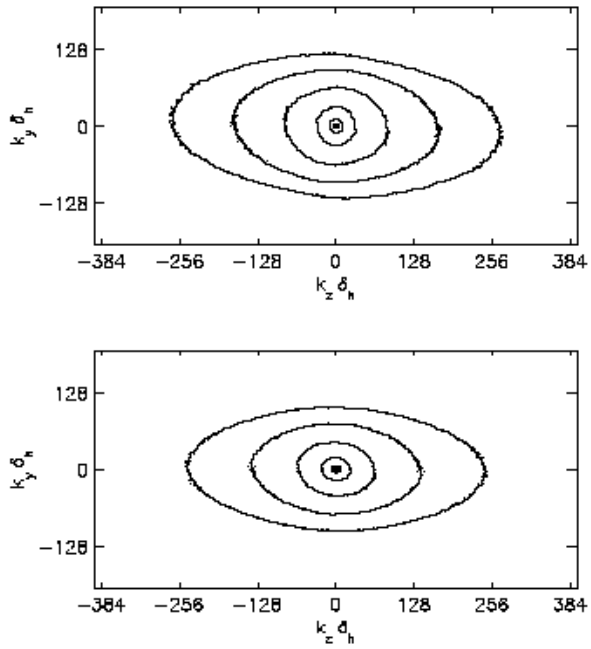

Figure 8 Two-dimensional power spectra of the scalar field of the transverse jet at $x / d_j = 50$. The wavenumber, k, is normalized by the local horizontal spatial extent, δ_h. Contour plots in $\log_{10}$ increments. Top: $Re = 1000$. Bottom: $Re = 10{,}000$ [6].

Figure 8 plots two-dimensional (spatial) scalar power spectra for a transverse jet, downstream of the injection station, at $x / d_j = 50$,

computed as an ensemble average of spatial spectra computed from a succession of frames, as in figure 7, for jet Reynolds numbers, $Re = 1000$ and 10,000 (jet-to-freestream speed ratio, $V_r = U_{jet} / U_\infty = 10$). Spatial-spectra contours are seen to be closer to circular (isotropic) for low wavenumbers, becoming increasingly elliptical at high wavenumbers. The reason, in this case, is traceable to the strain-rate field imposed on the small scales by the large-scale, streamwise vortices that dominate the far-field flow of transverse jets, owing to the large-scale streamwise vortices induced by the transverse injection. At least for this flow, the opposite behavior to the usual expectation can occur, *i.e.*, increasing anisotropy with increasing wavenumber.

This is illustrated in figure 9, which depicts a space-time image of a scalar field isosurface, *i.e.*, $c\,(y, z, t; x = 50\,d_j)$, compiled from a sequence of transverse cuts, recorded at a sufficiently high framing rate to meet the temporal Nyquist criterion for reconstructing the three-dimensional slice of the $c\,(x, y, z, t)$ data.

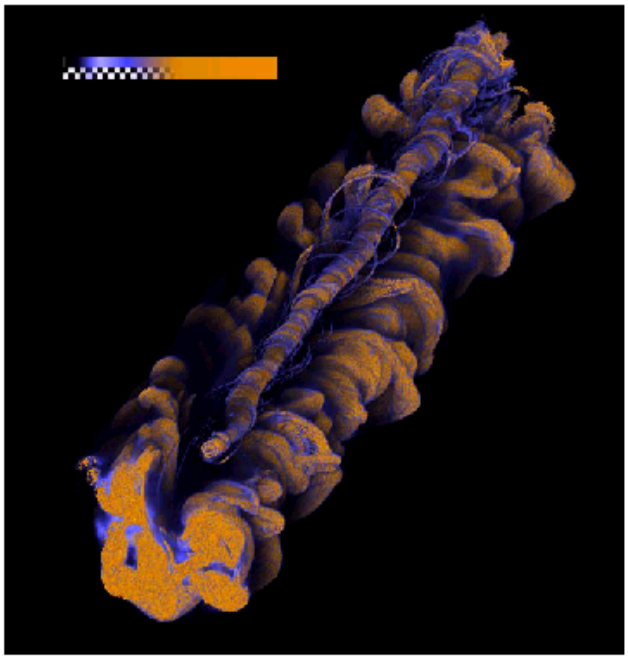

Figure 9 Three-dimensional, space-time visualization of an outer isosurface of jet-fluid concentration for a $Re = 1000$, $V_r = 10$, transverse jet, at $x/d_j = 50$. Time runs along the axis of the vortices. Visualization was computed in collaboration with S. Lombeyda of Caltech's CACR [6].

At this Reynolds number ($Re = 1000$), a small vortex is also evident, which is responsible for the left-right asymmetry in the flow and the slight tilt in the low-*Re* spatial spectrum (figure 8, top). At higher Reynolds numbers, only two counter-rotating ("kidney") vortices appear, generating a spanwise symmetric mean flow about the streamwise plane of symmetry that contains the jet nozzle, and untilted elliptical contours of the spatial spectrum (figure 8, bottom).

Compressibility effects

An emerging issue in turbulence is compressibility, or Mach number effects on the structure and dynamics of the flow. These can be scaled in terms of the so-called turbulence Mach number, $M_t = u' / a$, where u' is the rms velocity. Little guidance in this regime derives from work to date, with scant experimental data to steer theoretical and modeling efforts. As both *Re* and M_t scale linearly with velocity magnitude, high-M_t flows are also, typically, high-*Re* flows, placing them further out of reach of direct numerical simulation.

Weak *Re* effects in mixing were documented in experiments on high-*Re* shear layers [11,13,14]. These are illustrated in figure 10 that plots the normalized chemical-product thickness, δ_p / δ [14]. It is clear that this phenomenon is complex and may not be representable by a single model, given the complex dependence of the flow on initial/inflow conditions [17].

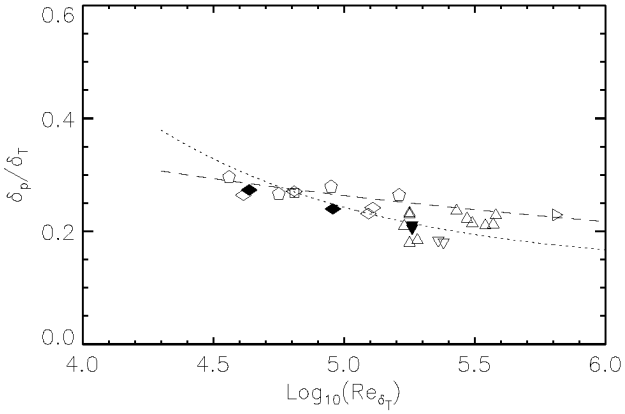

Figure 10 Shear-layer chemical product thickness vs. *Re* [14]. Dashed line: Dimotakis model [15]. Dotted line: Broadwell, Breidenthal, and Mungal model [16]. Initial splitter-plate boundary layers are estimated to be laminar for $Re < 10^5$ and turbulent for $Re > 3\times10^5$, or so [14, 17].

Figure 11 Rayleigh-scattering images of high-*Re* shear layers [18]. Top: Low-compressibility flow ($M_c = 0.15$), $U_1 = 200$ m/s [N_2], $U_2 = 100$ m/s [C_2H_4]. Bottom: High-compressibility flow (M_c=0.96), $U_1 = 1150$ m/s [He], $U_2 = 100$ m/s [C_2H_4].

Experiments designed to discriminate between Reynolds number from Mach number effects indicate that these effects are distinct and responsible for different mixing regimes [13]. This conclusion is also corroborated by laser Rayleigh-scattering measurements in high-speed shear layers [18]. Two images from those experiments are reproduced in figure 11. Compressibility is here quantified in terms of the (total) convective Mach number [19, 20],

$$M_c = \frac{U_1 - U_2}{a_1 + a_2}, \tag{4}$$

where U_1 and U_2 are the high- and low-speed freestream velocities, and a_1 and a_2 the high- and low-speed freestream speeds of sound.

Figure 11, top, is a low-compressibility flow, $M_c = 0.15$, with N_2 the high-speed freestream gas and C_2H_4 (ethylene) the low-speed freestream gas. These are density-matched but have different Rayleigh-scattering cross sections, permitting molecular-scattering images of thin slices to be recorded. The image on the bottom is from a supersonic high-speed freestream shear layer, with $M_c = 0.96$, helium as the high-speed freestream gas, and C_2H_4 the low-speed freestream gas.

The values quoted for M_c are useful for scaling and comparison purposes. Better estimates are based on the actual convection velocity of the large-scale turbulent structures, U_c, and are defined with respect to each of the free streams, *i.e.* [21],

$$M_{c1} = \frac{U_1 - U_c}{a_1}, \quad M_{c2} = \frac{U_c - U_2}{a_2}. \tag{5}$$

By way of example, at the supersonic flow conditions in the bottom image of figure 11, the large-scale-structure convection velocity is close to that of the high-speed freestream speed [11] and yields an estimate of $M_{c2} \approx 2.4$, in accord with the inclination angle of the (weak) oblique waves emanating from the turbulent zone into the low-speed freestream [18]. Since the rms velocity fluctuation, u', scales with the shear velocity, $\Delta U_i = |U_c - U_i|$, the turbulence Mach number, M_t, for this flow scales with $(M_{ci})_{max}$, the higher of the two convective Mach numbers, with values that can be estimated to be in the range, $M_t / (M_{ci})_{max} \approx 0.1 - 0.3$, with the lower values expected with increasing Mach number.

At low compressibility (figure 11, top), well-defined interfaces can be seen to mark the boundary between almost homogenized mixed fluid and unmixed freestream fluid. For high-compressibility flow (figure 11, bottom), mixed-fluid compositions are not as uniform. Oblique shocks, generated by supersonic relative convection speeds of the turbulent structures (M_{ci}'s comparable to, or greater than, unity), interact with the turbulence, generate baroclinic vorticity, and provide additional mixing and kinetic energy dissipation mechanisms. Not much is known about mixing in this flow regime, with experiment and theory indicating that while shear-layer growth is lower than for incompressible shear layers, the mixed-fluid fraction within the turbulent shear-layer region is higher [17, 22].

Modeling and simulation

Accepting the mixing transition as a common characteristic of most turbulent flows highlights the need for detailed, multi-dimensional measurements and direct numerical simulations to help guide theory and modeling for post-mixing-transition turbulent flows. The modal dimensionality of turbulence dictated by the minimum Reynolds number required for *bona fide* turbulence makes it unrealistic to expect that direct solutions of the Navier-Stokes equations can be relied upon to probe fully developed turbulence, and has been amply noted in the literature. It is also illustrated here by the computational effort required for the RTI Case D run. At least for flows with large density variations, DNS with $Re_h > 10^4$ must wait for the next generation of computing machinery. Similar challenges face the experimentalist, if fully resolved data are to be provided to guide model development.

On the positive side, experimental evidence suggests that flow Reynolds number is a strong parameter in pre-mixing-transition regimes, but only a weak parameter in fully developed turbulence, at least away from walls. In that regime, judicious Sub-Grid Scale (SGS) models may have a hope of capturing unresolved dynamics by augmenting Large Scale Eddy Simulations (LES). Nevertheless, one should bear in mind that the goal is to represent the notional zoomed inset in figure 1, right, given a coarsely resolved representation that has hopefully correctly captured the large-scale features of the flow represented in figure 1, left.

Turbulent mixing, which is dominated by small-scale behavior, presents a particular challenge. In many situations where the issue is the turbulent mixing itself, special experimental techniques, or theoretical and computational models must be employed to address it. In others, such as Rayleigh-Taylor instability that is driven by density inhomogeneities, a correct description of mixing is required to capture even the growth of the RTI mixing zone. Significant differences are reported depending on the details of explicit and implicit modeling and numerics. As Glimm *et al*. [23] note, "differences in numerical dissipation effects (mass diffusion and viscosity) due to algorithmic differences and differences in simulation duration are the dominant factors that produce such different results."

Particularly encouraging are recent SGS proposals by Pullin *et al*. [24-27] for incompressible, uniform-density turbulent flow. These assume that the dynamics below resolved spatial scales and associated sub-grid stresses are well represented by stretched spiral vortices of the type proposed by Lundgren [28]. These vortices are solutions of the N-S equations and generate a –5/3 velocity spectrum. These SGS models do not assume isotropy and exhibit a mixing transition at $Re_T \approx 100$ [26], even though there is nothing in the structure of the SGS model to have anticipated this. More recently, they were successfully extended to capture the scalar spectrum behavior for scalar fields with $Sc > 1$ [27].

Modeling compressible, non-uniform flows, especially turbulent flows with shocks, must be regarded as a current and challenging research topic. Many attempts to date have relied on *ad hoc* closures of the Euler equations with a variety of explicit or implicit numerical dissipation schemes. While many gasdynamic phenomena, especially ones dealing with shock propagation in uniform media, can be captured by such methods, strong shock-turbulence interactions and simulations represent as yet unchartered territory.

Conclusions

Recent experimental and numerical-simulation results have elucidated issues in turbulent mixing and also point to significant challenges yet to be addressed. New and developing experimental techniques that can record multi-dimensional spatio-temporal data, as well as the inexorable progress of direct-numerical simulations are guiding a new level of understanding and modeling, and can be expected to lead to further progress in the offing.

Acknowledgments

I would like to acknowledge discussions and the continuing collaboration on Rayleigh-Taylor instability flows with A. Cook, S. J. Chapman, and T. Mattner, as well as with D. Meiron, D. Pullin, and others in the Caltech ASCI/ASAP Compressible Turbulence group. This discussion and the recent experimental

and computational work reviewed was supported by AFOSR grants F49620–98–1–0052, F49620–00–1–0036, and F49620–01–1–0006, and DOE contract W–7405–ENG–48, which are gratefully acknowledged. Finally, I would like to thank the organizers of this conference for their invitation to attend and contribute to the proceedings.

References

[1] Kolmogorov, A. N. 1941. Local structure of turbulence in an incompressible viscous fluid at very high Reynolds numbers. *Akademiia Nauk SSSR Doklady* **30**, 301-305.

[2] Batchelor, G. K. 1959. Small-scale variation of convected quantities like temperature in turbulent fluid. Part I. General discussion and the case of small conductivity. *J. Fluid Mech.* **5**, 113-133.

[3] — 1968 *Los Angeles* (Sunset Lane, Menlo Park, CA), 246-247.

[4] Dimotakis, P. E., and Catrakis, H. J. 1999 Turbulence, fractals, and mixing. *Mixing: Chaos and Turbulence* (Kluwer Academic/Plenum Publishers, New York, NY), 59–143.

[5] Dimotakis, P. E. 2000 The mixing transition in turbulence. *J. Fluid Mech*. **409**, 69–98.

[6] Shan, J. W., and Dimotakis, P. E. 2001 Turbulent mixing in liquid-phase transverse jets. GALCIT Report, http://resolver.library.caltech.edu/CaltechGalcitFM:2001.006

[7] Cook, A. W., and Dimotakis, P.E. 2001 Transition stages of Rayleigh-Taylor instability between miscible fluids. *J. Fluid Mech*. **443**, 69–99, and continuing work in progress.

[8] Cook, A. W., Dimotakis, P. E., Chapman, S. J., and Mattner, T.W. 2001 Corrigendum: Transition stages of Rayleigh-Taylor instability between miscible fluids (in preparation).

[9] Duff, R. E., Harlow, F. H., and Hirt, C. W. 1962 Effects of Diffusion on Interface Instability Between Gases. *Phys. Fluids* **5**, 417–425.

[10] Dimonte, G., and Schneider, M. 2000 Density ratio dependence of Rayleigh-Taylor mixing for sustained and impulsive acceleration histories. *Phys. Fluids* **12**, 304–321.

[11] Dimotakis, P.E. 1991 Turbulent Free Shear Layer Mixing and Combustion. *High Speed Flight Propulsion Systems*, in *Prog. Astronautics and Aeronautics* **137**, Ch. 5, 265–340. In reference to RTI mixing, see Fig. 21, corresponding to $\delta_p(\xi=0.5)/\delta$ in that notation.

[12] Kang, H. S. and Meneveau, C. 2001 Passive scalar anisotropy in a heated turbulent wake: new observations and implications for large-eddy simulations. *J. Fluid Mech*. **442**, 161–170.

[13] Slessor, M. D. 1998 *Aspects of turbulent-shear-layer dynamics and mixing*. Ph.D. thesis, California Institute of Technology.

[14] Bond, C. L. 1999 *Reynolds Number Effects on Mixing in the Turbulent Shear Layer*. Ph.D. thesis, California Institute of Technology.

[15] Dimotakis, P. E. 1989 Turbulent shear layer mixing with fast chemical reactions. *Turbulent Reactive Flows. Lecture Notes in Engineering* **40** (Springer-Verlag, New York), 417–485.

[16] Broadwell, J. E., and Breidenthal, R. E. 1982 A simple model of mixing and chemical reaction in a turbulent shear layer. *J. Fluid Mech*. **125**, 397–410. Broadwell, J. E., and Mungal, M. G. 1991 Large-scale structures and molecular mixing. *Phys. Fluids* A **3**(5, Pt. 2), 1193–1206.

[17] Slessor, M. D., Bond, C. L., and Dimotakis, P. E. 1998 Turbulent shear-layer mixing at high Reynolds numbers: effects of inflow conditions. *J. Fluid Mech*. **376**, 115–138.

[18] Dimotakis, P. E., Catrakis, H. J., and Fourguette, D. C. 2001 Flow structure and optical beam propagation in high Reynolds number, gas-phase shear layers and jets. *J. Fluid Mech*. **433**, 105–134.

[19] Papamoschou, D. 1989 Structure of the compressible turbulent shear layer. AIAA Paper 89-0126.

[20] Slessor, M. D., Zhuang, M., and Dimotakis, P. E. 2000 Turbulent shear-layer mixing: growth-rate compressibility scaling. *J. Fluid Mech*. **414**, 35–45.

[21] Papamoschou, D., and Roshko, A. 1988 The Compressible Turbulent Shear Layer: An Experimental Study. *J. Fluid Mech*. **197**, 453–477.

[22] Hall, J. L., Dimotakis, P. E., and Rosemann, H. 1991 Some measurements of molecular mixing in compressible turbulent mixing layers. AIAA Paper 91–1719.

[23] Glimm, J., Grove, J. W., Li, X. L., Oh, W., and Sharp, D. H. 2001 A Critical Analysis of Rayleigh–Taylor Growth Rates. *J. Comp. Physics* **169**, 652–677.

[24] Pullin, D. I., and Saffman, P. G. 1994 Reynolds stresses and one-dimensional spectra for a vortex model of homogeneous anisotropic turbulence. *Phys. Fluids* **6**, 1787–1796.

[25] Misra, A. and Pullin, D. I. 1997 A vortex-based subgrid stress model for large-eddy simulation. *Phys. Fluids* **9**, 2443–2454.

[26] Pullin, D. I. 2000 A vortex-based model for the subgrid flux of a passive scalar. *Phys. Fluids* **12**, 2311–2319.

[27] Pullin, D. I. and Lundgren, T. S. 2001 Axial motion and scalar transport in stretched spiral vortices. *Phys. Fluids* **13**, 2553–2563.

[28] Lundgren, T. S. 1982 Strained spiral vortex model for turbulent fine structure. *Phys. Fluids* **25**, 2193–2203.